Charge transfer of slow highly charged xenon ions in collisions with magnesium atoms

W. Chen,[1,*] G. Vorobyev,[1] D. Guo,[2] P.-M. Hillenbrand,[1] F. Herfurth,[1] S. Hagmann,[1] U. Spillmann,[1] S. Trotsenko,[3] A. Gumberidze,[1,4] and Th. Stöhlker[1,3]

[1]*GSI Helmholtzzentrum für Schwerionenforschung, 64291 Darmstadt, Germany*

[2]*Institute of Modern Physics, Chinese Academy of Sciences, Lanzhou, 730000, Gansu, China*

[3]*Helmholtz-Institut Jena, Fröbelstieg 3, 07743 Jena, Germany*

[4]*ExtreMe Matter Institute EMMI and Research Division, GSI Helmholtzzentrum für Schwerionenforschung, 64291 Darmstadt, Germany*

(Received 5 September 2013; published 7 November 2013)

We report an experimental study of the charge-transfer process in collisions of Xe^{q+} ions ($16 \leqslant q \leqslant 20$) with magnesium atoms at an energy of $5.5q$ keV. With charge-selective and time-coincidence techniques, we separated the pure capture and capture accompanied by transfer-ionization processes. The experimental data indicate that the magnesium target is around two times more likely to lose two electrons than one in the collision. This finding is very different compared to the calculation based on the extended classic over-the-barrier model. The Xe^{q+}-Mg collision also behaves very differently from "traditional" collisions between highly charged ions and noble gases. We suggest a one-step dielectronic mechanism for the capture process. The data also show that autoionization dominates the relaxation process after the capture, and fluctuation of the autoionization fraction versus the projectile charge state indicates that for the relaxation processes, the projectile core structure plays a more important role than the detailed characteristics of the projectile states where the target electrons are initially captured.

DOI: 10.1103/PhysRevA.88.052703 PACS number(s): 34.70.+e

I. INTRODUCTION

Charge transfer is a fundamental atomic process which has been studied in various contexts for a long time, not only because it gives lot of information about atomic structure [1–5], but also because it plays an important role in astrophysics, fusion plasmas, and accelerator physics. For example, it is an important source of cometary and interstellar x rays [6,7]. Charge transfer also contributes as a powerful diagnostic tool in confined fusion plasmas [8]. In accelerator physics, charge transfer between highly charged ions (HCIs) and residual gas determines the lifetime of ion beams [9–11].

One of the well-known models used to describe capture processes for low-energy collisions is the extended classic over-the-barrier model (ECOB) [12]. In this model, the active electrons experience a Coulomb force from both the projectile and target nucleus. When the projectile approaches the target at a distance where the barrier is low enough for an electron to go from the target to the projectile, the electron is captured. The sequence of electron removal is determined by the target ionization potential. The ECOB model was later modified by Niehaus [2] and is currently known as the molecular Coulombic barrier model (MCBM). This model takes into consideration the probability of electrons staying in the target or being transferred to projectile ions during the quasimolecular state. ECOB and MCBM were verified and compared with many experimental results [13–15]. For collisions at medium and high energies where impact ionization occurs [16,17], different models were developed to describe the mechanism, such as the classic trajectory Monte Carlo model (CTMC) [18]. Apart from classic models, models based on the time-dependent two-center Dirac equation have recently been developed by Tupitsyn *et al.* [19,20] and provide good agreement with the experimental data [21].

Most of the experiments carried out in the past focus on charge transfer between ions and gaseous targets. Measurements of total charge exchange [22–25], recoil production [13–15,26–28], Auger electrons [29–32], photon emission [33–35], and their coincidence have been reported. Groh *et al.*'s measurement [36] shows that at sufficiently low energy, transfer ionization [see Eq. (1)] exceeds the electron-capture process in He^{2+}-Ar collisions. Another result from [26] indicates that the charge-state fractions do not depend explicitly on the projectile ion species and initial charge state, but rather upon the energy defect (change of system energy before and after the collision) of the system. DuBois measured [37] protons and He^{+} in collision with different targets as a function of projectile energy and pointed out the importance of transfer ionization in the low-energy collisions and of direct ionization channels for high-energy collisions. Cederquist *et al.* [38] reported direct ionization in low-energy Xe^{q+}-Xe collision with the variation of projectile charge q. The result exhibits an onset of ionization around $q = 13$ and follows approximate q^2 behavior at higher q, but the ionization process is still two orders of magnitude smaller than the capture process. The absolute cross sections of Xe^{q+}-(He, Ar, Xe) collisions were measured by Selberg *et al.* [14]. Based on a large data set, they proposed a set of semiempirical scaling laws [39], which also give a good agreement with other HCI-gas measurements [15,40].

Among HCI-gas collisions, the HCI-He system is of great interest because the electron-electron interaction plays an important role in the state-population dynamics during the capture process [22,28,41–43]. Based on a set of historical data, Frémont *et al.* [42] found that at low collision velocities, dielectronic processes favor the production of nonequivalent electron configurations because of the electron-electron interaction. To further investigate the electron-electron interaction in this process, it is interesting to use alkaline-earth metals because they have two loosely bound s^2 electrons outside a closed shell, making them He-like targets. This may induce different behaviors that help improve the understanding of the

*w.chen@gsi.de

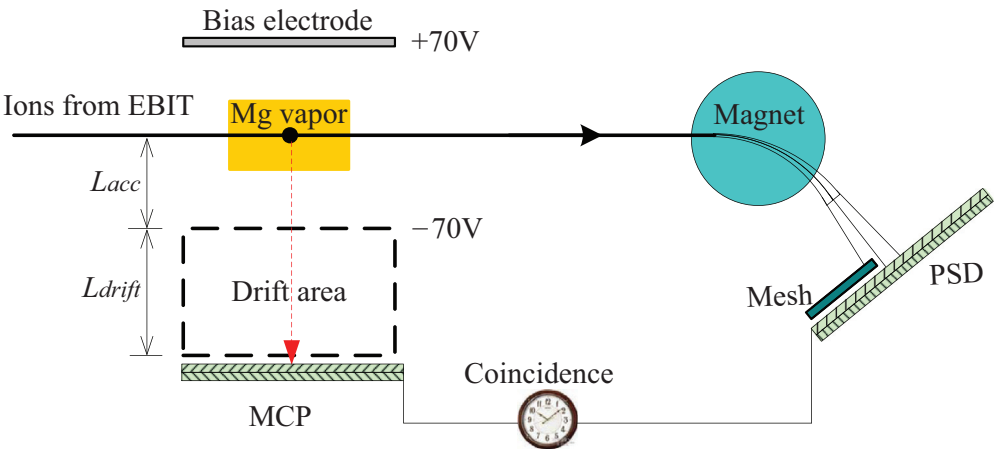

FIG. 1. (Color online) Schematic view of the experimental setup.

charge-transfer process. Martin *et al.* [34] studied the double-electron capture in slow collisions of bare ions from C^{6+} to Al^{13+} with gases from He to Xe and metallic vapor (strontium, barium, zinc) targets. They found that the population of asymmetrical configurations ($n,n' \gg n$) is responsible for the high radiative stabilization ratios.

In this work, we study the charge-transfer process between slow, highly charged xenon ions and magnesium atoms. The general process can be described as

$$\mathrm{Xe}^{q+} + \mathrm{Mg} \rightarrow \mathrm{Xe}^{(q-p)+} + \mathrm{Mg}^{r+} + (r-p)e^{-}. \qquad (1)$$

The corresponding cross section is indicated as $\sigma_r^{q,q-p}$. A condition $r - p = 0$ indicates a pure capture process, while $r - p > 0$ indicates a transfer-ionization (TI) process. In a more detailed description, the charge-transfer process has two steps: first, the projectile ion and target atom form a quasimolecule at the same time the projectile captures one or more electrons from the target to the projectile's ground or excited levels; second, the excited ions release energy by radiative decay or Auger processes. For Xe^{q+}-Mg collisions the double-electron transfer can be formulated as

$$\begin{aligned} \mathrm{Xe}^{q+} + \mathrm{Mg} &\rightarrow \mathrm{Xe}^{(q-2)+**}(nl,n'l') + \mathrm{Mg}^{2+}, \\ \text{radiative decay} &\rightarrow \mathrm{Xe}^{(q-2)+} + \mathrm{Mg}^{2+} + \gamma, \\ \text{autoionization} &\rightarrow \mathrm{Xe}^{(q-1)+} + \mathrm{Mg}^{2+} + e^{-}, \end{aligned} \qquad (2)$$

in which nl indicates the inner electron and $n'l'$ indicates the outer electron, i.e., $n' \geqslant n$.

II. EXPERIMENT

The schematic view of the experimental setup is shown in Fig. 1. The highly charged xenon ions ($^{132}Xe^{q+}$) were extracted from the electron-beam ion trap at GSI (SPARC-EBIT [44]) with an energy of $5.5q$ keV. The EBIT was running in a so-called leaky mode; that is, the ions were extracted continuously. After passing through by a charge-selective bending magnet, the ion beam collided with a collimated magnesium vapor jet produced by an oven. At saturated pressure the vapor is composed of only monomers, having a fraction of dimers (Mg_2) of only 0.004% [45]. At room temperature, the vapor pressure of magnesium is less than 10^{-10} Torr [46]. Therefore, the differential pump system usually used with gas targets is not necessary here. Finally, the projectiles were dispersed by another bending magnet to separate the primary beam and charge-exchanged ions, both of which were recorded by a position-sensitive detector in coincidence with a recoil ion. The recoils (Mg^{r+}) were first accelerated in the electric field produced by a biased electrode and a mesh and then passed through a field-free drift region before being detected. The charge states of the recoils were separated by time-of-flight (TOF) measurements. For better TOF resolution, this was arranged in a configuration such that the acceleration distance L_{acc} was one half the drift distance L_{drift}. A typical position spectrum from the projectile detector and a coincident TOF spectrum from the recoil detector are shown in Figs. 2 and 3.

Both the projectile and recoil detectors were microchannel plates (MCP) from RoentDek. They were covered with nearly transparent grids, which had negative voltage relative to the MCP front surfaces to maximize the detection efficiency [47,48]. The MCP for the projectile detection had a delay

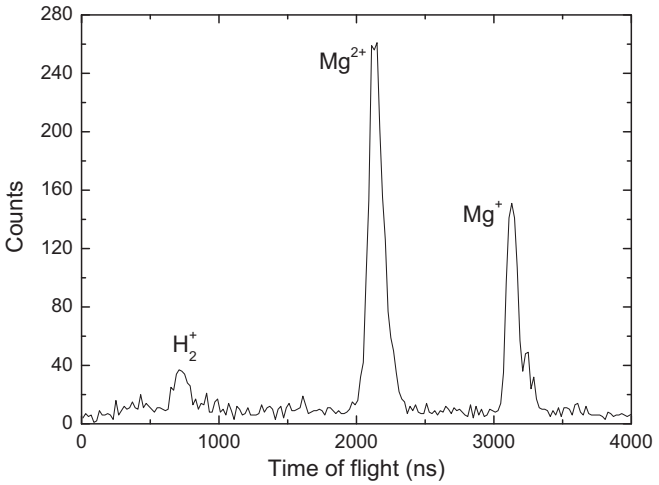

FIG. 2. TOF spectrum of the recoils with a projectile as the trigger start. Mg^{+} and Mg^{2+} were produced in the charge-transfer processes. Production of Mg^{3+} recoils could not be observed. H_2^+ is from Xe^{q+} collisions with a background gas, mainly hydrogen from the reaction of H_2O that attached on the chamber surface and Mg atom.

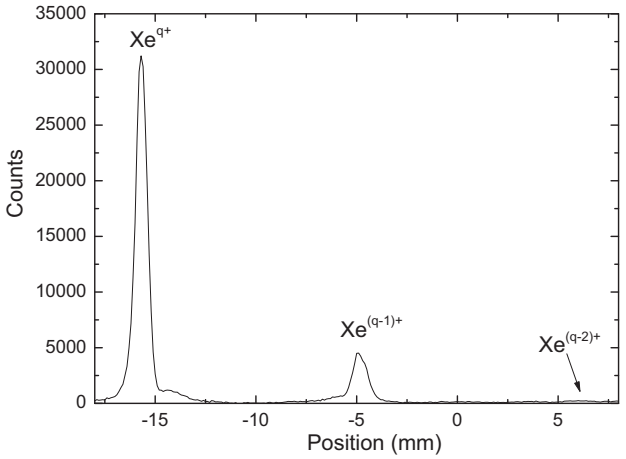

FIG. 3. Charge-state distribution of the projectile ions after collisions with the magnesium target. The primary beam Xe^{q+} is attenuated by a dense mesh (around 1.3% transparency) in front of the position-sensitive detector. Although $Xe^{(q-2)+}$ ions are more than one order of magnitude less than $Xe^{(q-1)+}$, they can be distinguished by applying a coincidence technique.

line anode to generate a position signal. A dense mesh with around 1.3% transparency covered part of the projectile detector. It attenuated the primary beam to less than 0.1% of the saturation limit of MCP. The particle energy dependence of the MCP quantum efficiency has been studied in many works [48–52]. They concluded that the quantum efficiency of MCP saturates and converges to a constant value when the particle energy exceeds a certain threshold. From our test, this value is around 3.3 keV for Mg^+ (see Fig. 4). For the highly charged xenon projectiles ($q \geqslant 8$), an energy of $5.5q$ keV is above the saturation threshold, and the energy loss during the collision is negligible. Therefore, the detection efficiencies for the projectiles and charge-exchanged ions are equal, and the detection efficiencies for different recoils are also equal.

We carried out the measurements for xenon ions with charge states $16 \leqslant q \leqslant 20$, where Xe^{18+} has a Kr-like shell. It is interesting to study the charge-transfer processes for this and the neighboring charge states because of the drastic change of the electron configurations of the projectile core.

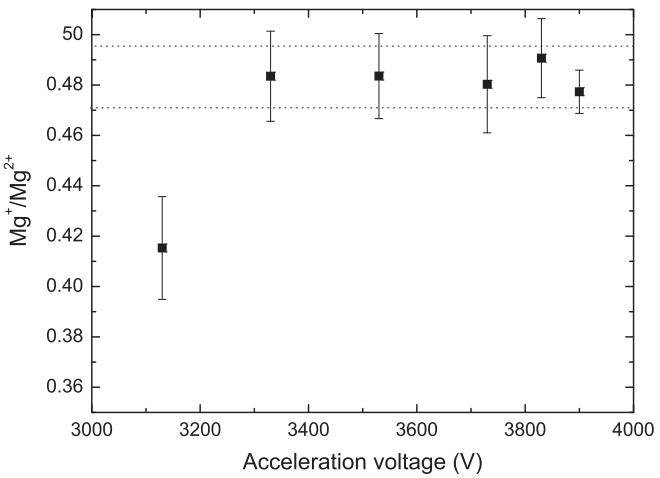

FIG. 4. The Mg^+/Mg^{2+} ratios vs acceleration voltage in the collisions of Xe^{20+} ions and magnesium vapor. This ratio converges to a constant when the acceleration voltage is higher than 3.3 kV, corresponding to the saturation threshold of the MCP.

III. RESULTS AND DISCUSSION

After appropriate background subtraction, the peak areas are proportional to the corresponding cross sections. Since the reaction investigated is exoergic and the impact velocity is low (∼0.2 a.u.), the cross section of the reaction is almost independent of the projectile energy within the range we studied [26]. Because of difficulties in determining the target density, it was not possible to obtain precise absolute cross sections in this study. Correspondingly, we were able to perform relative cross-section measurements, and they give quite different results from those obtained in collisions between HCIs and different gaseous targets.

A. Ratios of electron-removal cross sections

The cross-section ratio of two-electron removal to one-electron removal from the target σ_2/σ_1 vs the projectile charge state is shown in Fig. 5. One can see that the target has a higher probability to lose two electrons than one, i.e., $\sigma_2/\sigma_1 > 1$. The ratio increases with the charge state of the projectile to a value of around 2.0 at $q = 20$. These results deviate significantly from predictions based on the ECOB model [12] as well as the calculation using the semiempirical formula given in Ref. [39]. Both calculations give values of less than 1, independently of the projectile charge state. Collisions of slow Xe^{q+} ($15 \leqslant q \leqslant 43$) with He, Ar, and Xe targets at velocities around 0.2 a.u. were investigated by Selberg *et al.* [14]. Their results showed that σ_2/σ_1 is always less than 1. This rule was verified in other HCI-gas collision measurements [13,15] and also in HCI-metallic-vapor collision [34], with a value of 0.7 in Ne^{10+}-Sr collision at a velocity around 0.2 a.u. Yet in our Xe^{q+}-Mg

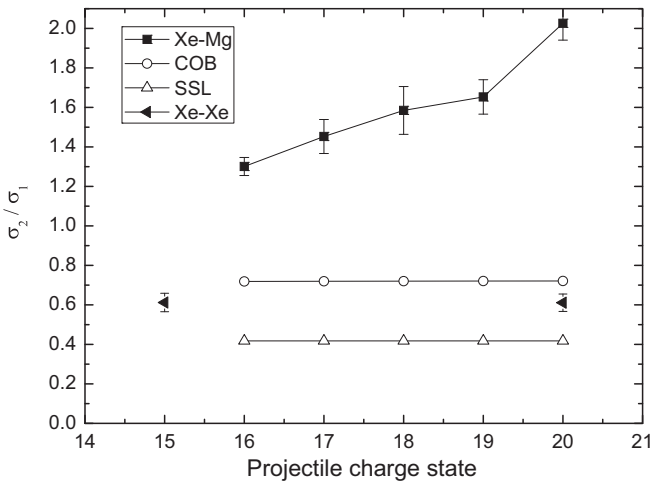

FIG. 5. The cross-section ratios of two- to one-electron removal vs the charge state of the projectile. The solid squares depict our measurement of Xe^{q+}-Mg collisions. The open circles are the calculations based on ECOB, and the open triangles show the calculations based on Selberg *et al.*'s semiempirical formula [39]. The solid triangles are the results from Selberg *et al.*'s Xe^{q+}-Xe collision measurements [14].

measurement the result is totally different from most of the other low-energy collisions, except for a few measurements with low charged projectiles, such as for C^{4+}-He [22,43] and He^{2+}-Ar [36] collisions. In those collisions the electrons are not captured to high Rydberg states because of the low-charge state of the projectiles, and crossings of the potential energy curves for the initial and final states play an important role.

One possible explanation of the different behavior is the dominance of the so-called *correlated double-electron capture* [31,41,42]. Chesnel *et al.* [31] considered two kinds of double-capture mechanisms denoted as *monoelectronic* and *dielectronic* processes. In monoelectronic process, the two active electrons are captured independently. The interaction between the two active electrons within the target ($3s^2$ for Mg) plays an important role. Once the first electron overcomes the Coulomb barrier and is captured by the projectile, the electron-electron interaction of the two $3s^2$ electrons will disappear, and thus, the ionization energy for the second electron will increase, corresponding to a higher barrier which reduces the probability of the second electron being captured. The state population of the two captured electrons mainly depends on the match between their ionization energies and the energy levels of the projectile, usually resulting in (near-)equivalent configurations. In the dielectronic process, the two electrons are captured simultaneously in one step but tend to create configurations of nonequivalent electrons (i.e., $|n - n'|$ is large), which indicates that the two electrons are correlated during the capture process [31,34,41]. The monoelectronic process is adopted in the over-the-barrier model. In this model, σ_2/σ_1 is always less than 1 because the barrier to remove the second electron is about two times higher than the barrier to remove the first one. Therefore, we believe in our experiment that the two $3s^2$ electrons of the magnesium atom are captured mainly via the dielectronic pathway. As the charge of the projectile increases, the electron-HCI interaction overwhelms the electron-electron interaction of the two $3s^2$ electrons, resulting in a higher possibility of the dielectronic process.

Frémont *et al.* [42] summarized HCI-He collisions with velocities in the range 0.1−0.5 a.u. and concluded that at low collision energies the dielectronic process dominates, whereas monoelectronic processes are enhanced as the projectile velocity increases. This conclusion was proven in different measurements [22,31] and calculations [53]. For Selberg *et al.*'s Xe^{q+}-(He, Ar, Xe) collisions [14] and Martin's HCI-(gas, metal vapor) collisions [34], the projectiles had almost the same velocity as in our Xe^{q+}-Mg collisions (∼0.2 a.u.), and there the monoelectronic process dominates the capture process, while in C^{4+}-He collisions [22] the dielectronic process starts to dominate when the velocity decreases down to around 0.3 a.u. We presume that whether the monoelectronic or dielectronic process dominates depends not only on the projectile velocity but also on the charge state of the projectile and the target species. The target dependence of σ_2/σ_1 for the same projectile and velocity is shown in Fig. 6, with the average ionization energy of the first electron and second electron as the x coordinate. The σ_2/σ_1 value decreases with increasing average ionization energy.

Furthermore, the TOF spectrum of recoil ions (see Fig. 2) shows no three-electron removal events. This could be explained by the rapid change of the ionization energy for the target atom while opening a closed shell. The ECOB model gives σ_3/σ_2 with a value around 2%, which is the statistical uncertainty range of our experiment. But the semiempirical scaling law by Selberg *et al.* [39] predicts a σ_3/σ_2 value around 5.6%, which should be observable in our TOF spectra. Therefore, this scaling law indeed seems to work only for removal of outer-shell electrons in HCI-gas collisions, as the paper defined.

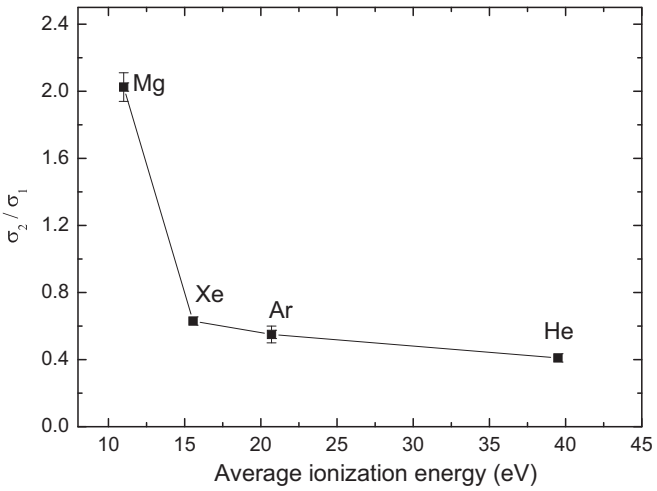

FIG. 6. Target dependence of σ_2/σ_1 in Xe^{20+}-(He, Ar, Xe, Mg) collisions with a velocity of ∼0.2 a.u. The Xe^{20+}-Mg data are from this work, and Xe^{q+}-(He, Ar, Xe) data are from Selberg *et al.*'s work [14], in which the Xe^{20+}-Ar value is extrapolated from a figure in their paper.

B. The ratio of two-electron capture to transfer-ionization cross sections

The cross-section ratio of two-electron capture to transfer ionization $\sigma_2^{q,q-2}/\sigma_2^{q,q-1}$ reflects the branching ratio between the two competitive relaxation channels after the two-electron-transfer process: radiative decay and autoionization. For radiative decay, the intershell electric dipole transition rate scales as q^4, while the Coulombic autoionization varies very slowly with q [27,54]. Consequently, $\sigma_2^{q,q-2}/\sigma_2^{q,q-1}$ increases with q in general. This tendency is also illustrated in Xe^{q+}-gas collision experiments [14,27].

The $\sigma_2^{q,q-2}/\sigma_2^{q,q-1}$ results for our experiment are shown in Fig. 7 together with other HCI-gas collision data. We can see that in all of the measurements the autoionization process dominates the relaxation process, but for Xe^{20+}-Mg collision, the $\sigma_2^{q,q-2}/\sigma_2^{q,q-1}$ value seems to be slightly higher on average. As discussed in Sec. III A, the two $3s^2$ electrons of magnesium are captured, presumably in a one-step dielectronic process, and tend to populate nonequivalent configurations with large $|n - n'|$. These asymmetric states ($n \ll n'$) were proved to enhance the probability of the radiative relaxation [33,34,56]. For the collisions that produce high Rydberg states with $n \geqslant 6$ (Xe^{20+}, I^{19+} in Fig. 7), the $\sigma_2^{q,q-2}/\sigma_2^{q,q-1}$ value increases with decreasing binding energy. Similar phenomena were also found by other groups [13,27,34]. For example, in HCI-Sr collisions [34], the target has a similar configuration to magnesium and has even smaller ionization energy. Consequently,

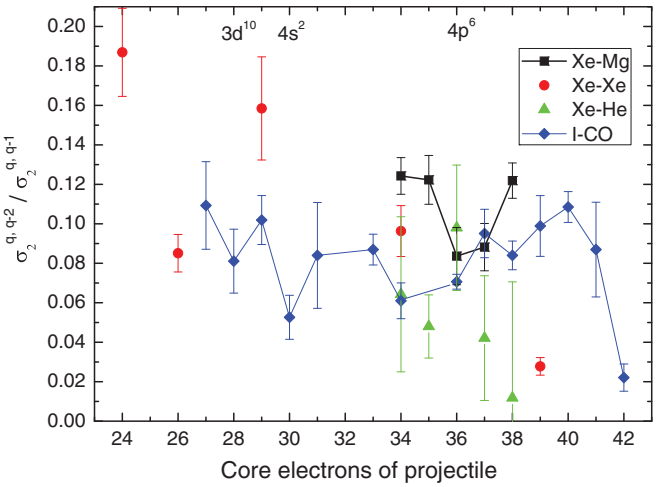

FIG. 7. (Color online) The cross-section ratios of the two-electron-capture to transfer-ionization process vs the number of core electrons of the projectile. Black squares are results for the Xe^{q+}-Mg collisions, the red solid circles show the results from Selberg *et al.*'s Xe^{q+}-Xe measurements [14], the green triangles indicate Xe^{q+}-He collisions from Andersson *et al.* [24], and blue diamonds indicate I^{q+}-CO collisions from Krok *et al.* [55].

it has a higher radiative decay percentage than the HCI-gas collisions with about the same projectile charge state.

Apart from the detailed characteristics of the initial-state population after the capture, the projectile core structure also plays an important role in the relaxation processes for high Rydberg states [27,55,57]. This leads to a nonmonotonous dependence of $\sigma_2^{q,q-2}/\sigma_2^{q,q-1}$ on q, although it is proved to increase with increasing q in general [27]. Based on a series of Q-value measurements and estimations of (n,n') in collisions of Xe^{q+}-He [14,58], I^{q+}-CO [55], Xe^{q+}-Xe [14,59], Xe^{q+}-Na [60], and HCI-metal [34], we summarize that the n value increases with decreasing binding energy of the target. The collisions of Xe^{q+}-Mg are estimated to produce populations of $8 \leqslant n \leqslant n'$, where the two Rydberg electrons are almost unaffected by the projectile core charge. The two electrons are presumed to stabilize through a yrast chain cascade ($E1$ transitions with $\Delta n \leqslant 1$). The core configuration of the projectile plays a critical role in the last step of the cascade chain [27,57]. For example, a closed subshell has a less statistic weight than a partially filled subshell (e.g., $2J+1$ in the L-S coupling scheme); consequently, it results in a lower possibility for radiative decay. This is one of the possible reasons why Xe^{18+}-Mg ($4p^6$ core) has a lower $\sigma_2^{q,q-2}/\sigma_2^{q,q-1}$ value than the neighboring charge states (see Fig. 7). A similar nonmonotonous dependence of $\sigma_2^{q,q-2}/\sigma_2^{q,q-1}$ on q was also investigated in I^{q+}-CO collisions [55], where low points were found at $3d^{10}$ and $4s^2$ configurations (possibly also for $4p^6$, but the data for $4p^5$ were not given).

C. Derivative ratios

Since direct ionization of the magnesium target is not likely for the velocity range we studied here and also almost no Mg^{3+} ions could be observed in our experiment, the ratio of double- to single-electron capture $\sigma^{q,q-2}/\sigma^{q,q-1}$ is strongly related to σ_2/σ_1 and $\sigma_2^{q,q-1}/\sigma_2^{q,q-2}$. Figure 8 shows the result of $\sigma^{q,q-2}/\sigma^{q,q-1}$ as a function of projectile charge. The double-electron-capture cross section is more than one order of magnitude smaller than that for one-electron capture, even though magnesium is more likely to lose two electrons. The nonmonotonous relationship indicates that not only charge but also the electron configuration of the projectile contributes to $\sigma^{q,q-2}/\sigma^{q,q-1}$. Another derivative ratio shown in Fig. 8 is $\sigma_2^{q,q-1}/\sigma_1^{q,q-1}$, which indicates that as the charge of the projectile increases, transfer ionization starts to contribute as a main source of the one-electron-capture process. On the contrary, in Xe^{q+}-He and Xe^{q+}-Xe collision, the single capture is mainly from a single charge transfer.

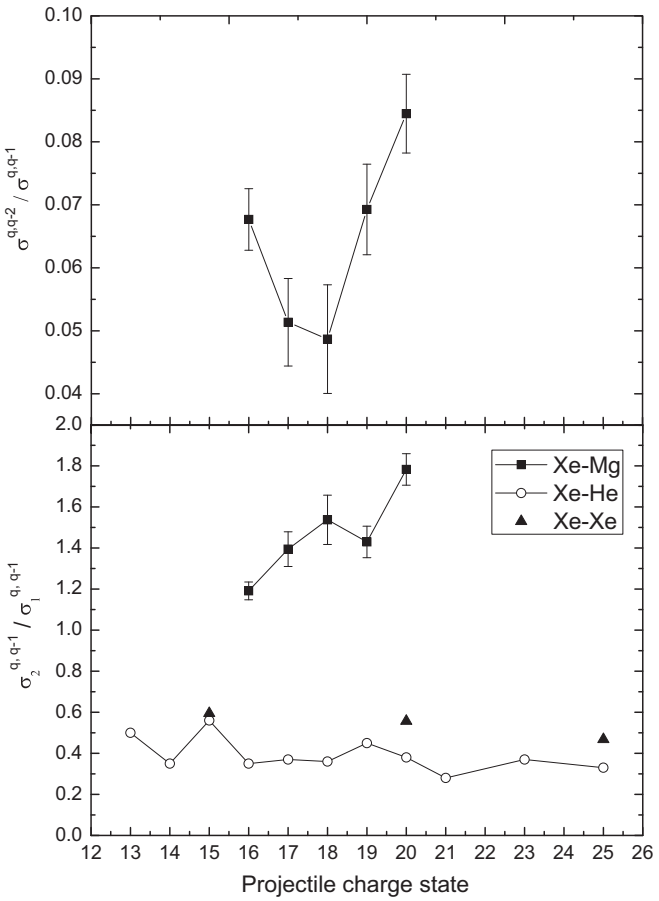

FIG. 8. Derivative ratios from σ_2/σ_1 and $\sigma_2^{q,q-2}/\sigma_2^{q,q-1}$. (top) Double- to single-electron capture; (bottom) one-electron capture from transfer ionization vs from pure capture, where solid squares indicate our Xe^{q+}-Mg collisions, solid triangles are Xe^{q+}-Xe collisions [14], and open circles show the Xe^{q+}-He collisions [24].

IV. CONCLUSION

We studied the charge-transfer process in Xe^{q+}-Mg collisions ($16 \leqslant q \leqslant 20$). With the position and the TOF information from the projectile and the target detectors, respectively, we obtained the cross-section ratios of two- to one-electron removal σ_2/σ_1 and the branching ratios of the radiative decay to autoionization $\sigma_2^{q,q-2}/\sigma_2^{q,q-1}$ in the projectile relaxation processes. The values of σ_2/σ_1 deviate significantly from the

calculation based on the ECOB model, in which the target electrons are captured independently in sequence. No three-electron removal events have been observed in the experiment, and correspondingly, no three-electron-capture processes take place. We compared our results with measurements from other groups, showing that Xe^{q+}-Mg collisions have quite different features from "traditional" HCI-gas collisions. So we speculate that a one-step dielectronic process [31,42] is responsible for the charge transfer. σ_2/σ_1 shows a strong dependence on the projectile charge, target species, and velocity [42]. The doubly excited Rydberg state mainly decays through autoionization, indicated by $\sigma_2^{q,q-2}/\sigma_2^{q,q-1}$ ratios. As the charge of the projectile increases, the $\sigma_2^{q,q-2}/\sigma_2^{q,q-1}$ value has an increasing tendency in general, but the electron configuration of the core gives a large contribution, which causes a fluctuation. The derivative ratios show that two-electron-capture probability is one order of magnitude smaller than that for one-electron capture, and the latter process mainly results from the two-electron-transfer process accompanied by autoionization.

To further study the dominance of the one-step dielectric process, we are going to increase the charge state of projectiles and carry out Q-value measurements to investigate the populated projectile states in detail. The device will also be improved for the precise absolute cross-section measurements.

ACKNOWLEDGMENTS

The authors gratefully acknowledge the support from the HITRAP and atomic physics groups of GSI and beneficial discussions with Deyang Yu from Lanzhou and Robert D. Dubois from Missouri University of Science and Technology.

[1] D. Basu, S. Mukherjee, and D. Sural, Phys. Rep. **42**, 145 (1978).
[2] A. Niehaus, J. Phys. B **19**, 2925 (1986).
[3] H. Ryufuku, K. Sasaki, and T. Watanabe, Phys. Rev. A **21**, 745 (1980).
[4] K. R. Cornelius, K. Wojtkowski, and R. E. Olson, J. Phys. B **33**, 2017 (2000).
[5] A. Surzhykov, S. Fritzsche, A. Gumberidze, and T. Stöhlker, Phys. Rev. Lett. **88**, 153001 (2002).
[6] S. Otranto, R. E. Olson, and P. Beiersdorfer, Phys. Rev. A **73**, 022723 (2006).
[7] K. Dennerl, Space Sci. Rev. **157**, 57 (2010).
[8] *Atomic and Plasma-Material Interaction Data for Fusion*, edited by R. Clark (International Atomic Energy Agency, Vienna, 2008), Vol. 13.
[9] V. Shevelko, O. Brinzanescu, W. Jacoby, M. Rau, and T. Stöhlker, Hyperfine Interact. **114**, 289 (1998).
[10] T. Stöhlker, T. Ludziejewski, H. Reich, F. Bosch, R. W. Dunford, J. Eichler, B. Franzke, C. Kozhuharov, G. Menzel, P. H. Mokler, F. Nolden, P. Rymuza, Z. Stachura, M. Steck, P. Swiat, A. Warczak, and T. Winkler, Phys. Rev. A **58**, 2043 (1998).
[11] V. Shevelko, I. Beigman, M. Litsarev, H. Tawara, I. Tolstikhina, and G. Weber, Nucl. Instrum. Methods Phys. Res., Sect. B **269**, 1455 (2011).
[12] A. Bárány, G. Astner, H. Cederquist, H. Danared, S. Huldt, P. Hvelplund, A. Johnson, H. Knudsen, L. Liljeby, and K.-G. Rensfelt, Nucl. Instrum. Methods Phys. Res., Sect. B **9**, 397 (1985).
[13] N. Nakamura, F. J. Currell, A. Danjo, M. Kimura, A. Matsumoto, S. Ohtani, H. A. Sakaue, M. Sakurai, H. Tawara, H. Watanabe, I. Yamada, and M. Yoshino, J. Phys. B **28**, 2959 (1995).
[14] N. Selberg, C. Biedermann, and H. Cederquist, Phys. Rev. A **56**, 4623 (1997).
[15] D. Yu, X. Cai, R. Lu, F. Ruan, C. Shao, H. Zhang, Y. Cui, J. Lu, X. Xu, J. Shao, B. Ding, Z. Yang, X. Chen, and Z. Liu, Phys. Rev. A **76**, 022710 (2007).
[16] H. Knudsen, L. H. Andersen, P. Hvelplund, J. Sørensen, and D. Ćirić, J. Phys. B **20**, L253 (1987).
[17] S. Datz, R. Hippler, L. H. Andersen, P. F. Dittner, H. Knudsen, H. F. Krause, P. D. Miller, P. L. Pepmiller, T. Rosseel, R. Schuch, N. Stolterfoht, Y. Yamazaki, and C. R. Vane, Phys. Rev. A **41**, 3559 (1990).
[18] R. E. Olson and A. Salop, Phys. Rev. A **16**, 531 (1977).
[19] I. I. Tupitsyn, Y. S. Kozhedub, V. M. Shabaev, G. B. Deyneka, S. Hagmann, C. Kozhuharov, G. Plunien, and T. Stöhlker, Phys. Rev. A **82**, 042701 (2010).
[20] I. I. Tupitsyn, Y. S. Kozhedub, V. M. Shabaev, A. I. Bondarev, G. B. Deyneka, I. A. Maltsev, S. Hagmann, G. Plunien, and T. Stöhlker, Phys. Rev. A **85**, 032712 (2012).
[21] S. Hagmann, S. Kelbch, H. Schmidt-Böcking, C. L. Cocke, P. Richard, R. Schuch, A. Skutlartz, J. Ullrich, B. Johnson, M. Meron, K. Jones, D. Trautmann, and F. Rösel, Phys. Rev. A **36**, 2603 (1987).
[22] D. H. Crandall, R. E. Olson, E. J. Shipsey, and J. C. Browne, Phys. Rev. Lett. **36**, 858 (1976).
[23] E. Justiniano, C. L. Cocke, T. J. Gray, R. Dubois, C. Can, W. Waggoner, R. Schuch, H. Schmidt-Böcking, and H. Ingwersen, Phys. Rev. A **29**, 1088 (1984).
[24] H. Andersson, G. Astner, and H. Cederquist, J. Phys. B **21**, L187 (1988).
[25] P. Hvelplund, S. K. Bjørnelund, H. Knudsen, and H. Tawara, Phys. Scr. **45**, 231 (1992).
[26] W. Groh, A. Müller, A. S. Schlachter, and E. Salzborn, J. Phys. B **16**, 1997 (1983).
[27] H. Cederquist, H. Andersson, E. Beebe, C. Biedermann, L. Broström, A. Engström, H. Gao, R. Hutton, J. C. Levin, L. Liljeby, M. Pajek, T. Quinteros, N. Selberg, and P. Sigray, Phys. Rev. A **46**, 2592 (1992).
[28] W. Wu, J. P. Giese, Z. Chen, R. Ali, C. L. Cocke, P. Richard, and M. Stöckli, Phys. Rev. A **50**, 502 (1994).
[29] S. Hagmann, S. Kelbch, C. L. Cocke, P. Richard, A. Skutlartz, H. Schmidt-Böcking, R. Schuch, B. Johnson, M. Meron, and K. Jones, Phys. Rev. A **34**, 2897 (1986).
[30] F. Fremont, H. Merabet, J. Y. Chesnel, X. Husson, A. Lepoutre, D. Lecler, G. Rieger, and N. Stolterfoht, Phys. Rev. A **50**, 3117 (1994).
[31] J.-Y. Chesnel, B. Sulik, H. Merabet, C. Bedouet, F. Frémont, X. Husson, M. Grether, A. Spieler, and N. Stolterfoht, Phys. Rev. A **57**, 3546 (1998).

[32] E. D. Emmons, A. A. Hasan, and R. Ali, Phys. Rev. A **60**, 4616 (1999).
[33] S. Martin, A. Salmoun, Y. Ouerdane, M. Druetta, J. Désesquelles, and A. Denis, Phys. Rev. Lett. **62**, 2112 (1989).
[34] S. Martin, J. Bernard, L. Chen, A. Denis, and J. Désesquelles, Phys. Scr. T **73**, 149 (1997).
[35] P. Beiersdorfer, M. Bitter, M. Marion, and R. E. Olson, Phys. Rev. A **72**, 032725 (2005).
[36] W. Groh, A. S. Schlachter, A. Müller, and E. Salzborn, J. Phys. B **15**, L207 (1982).
[37] R. D. DuBois, Phys. Rev. A **34**, 2738 (1986).
[38] H. Cederquist, C. Biedermann, N. Selberg, E. Beebe, M. Pajek, and A. Bárány, Phys. Rev. A **47**, R4551 (1993).
[39] N. Selberg, C. Biedermann, and H. Cederquist, Phys. Rev. A **54**, 4127 (1996).
[40] S. Madzunkov, D. Fry, and R. Schuch, J. Phys. B **37**, 3239 (2004).
[41] N. Stolterfoht, C. Havener, R. Phaneuf, J. Swenson, S. Shafroth, and F. Meyer, Nucl. Instrum. Methods Phys. Res., Sect. B **27**, 584 (1987).
[42] F. Frémont, C. Bedouet, X. Husson, and J.-Y. Chesnel, Phys. Rev. A **57**, 4379 (1998).
[43] M. Hoshino, L. Pichl, Y. Kanai, Y. Nakai, M. Kitajima, M. Kimura, Y. Li, H.-P. Liebermann, R. J. Buenker, H. Tanaka, and Y. Yamazaki, Phys. Rev. A **75**, 012716 (2007).
[44] A. Sokolov, F. Herfurth, O. Kester, T. Stoehlker, A. Thorn, G. Vorobjev, and G. Zschornack, J. Instrum. **5**, C11001 (2010).
[45] Z. Slania, Thermochim. Acta **207**, 9 (1992).
[46] V. Klyuev, V. Parkhomchuk, and S. Rastigeev, Instrum. Experim Tech. **52**, 245 (2009).
[47] R. C. Taylor, M. C. Hettrick, and R. F. Malina, Rev. Sci. Instrum. **54**, 171 (1983).
[48] R. S. Gao, P. S. Gibner, J. H. Newman, K. A. Smith, and R. F. Stebbings, Rev. Sci. Instrum. **55**, 1756 (1984).
[49] J. Oberheide, P. Wilhelms, and M. Zimmer, Meas. Sci. Technol. **8**, 351 (1997).
[50] S. Yagi, T. Nagata, M. Koide, Y. Itoh, T. Koizumi, and Y. Azuma, Nucl. Instrum. Methods Phys. Res., Sect. B **183**, 476 (2001).
[51] E. Liénard, M. Herbane, G. Ban, G. Darius, P. Delahaye, D. Durand, X. Fléchard, M. Labalme, F. Mauger, A. Mery, O. Naviliat-Cuncic, and D. Rodrguez, Nucl. Instrum Methods Phys. Res., Sect. A **551**, 375 (2005).
[52] N. Takahashi, S. Hosokawa, M. Saito, and Y. Haruyama, Phys. Scr. **2011**, 014057 (2011).
[53] J. P. Hansen, J. Phys. B **25**, L17 (1992).
[54] R. Janev and L. Presnyakov, Phys. Rep. **70**, 1 (1981).
[55] F. Krok, I. Y. Tolstikhina, H. A. Sakaue, I. Yamada, K. Hosaka, M. Kimura, N. Nakamura, S. Ohtani, and H. Tawara, Phys. Rev. A **56**, 4692 (1997).
[56] J.-Y. Chesnel, H. Merabet, B. Sulik, F. Frémont, C. Bedouet, X. Husson, M. Grether, and N. Stolterfoht, Phys. Rev. A **58**, 2935 (1998).
[57] R. Ali, C. L. Cocke, M. L. A. Raphaelian, and M. Stockli, J. Phys. B **26**, L177 (1993).
[58] H. Cederquist, C. Biedermann, N. Selberg, and P. Hvelplund, Phys. Rev. A **51**, 2191 (1995).
[59] H. Anderson, H. Cederquist, G. Astner, P. Hvelplund, and J. O. P. Pedersen, Phys. Scr. **42**, 150 (1990).
[60] V. G. Hasan, S. Knoop, R. Morgenstern, and R. Hoekstra, J. Phys. Conf. Ser. **58**, 199 (2007).